$LaPO_4$ Mineral Liquid Crystalline Suspensions with Outstanding Colloidal Stability for Electro-Optical Applications

Jongwook Kim, Alexis de la Cotte, Rodolphe Deloncle, Samuel Archambeau, Claudine Biver, Jean-Paul Cano, Khalid Lahlil, Jean-Pierre Boilot, Eric Grelet, and Thierry Gacoin**

Mineral liquid crystals are materials in which mineral's intrinsic properties are combined with the self-organization behavior of colloids. However, the use of such a system for practical application, such as optical switching, has rarely been demonstrated due to the fundamental drawbacks of colloidal systems such as limited dispersion stability. Studying colloidal suspensions of $LaPO_4$ nanorods, it is found that drastic improvement of colloidal stability can be obtained through a transfer of particles from water towards ethylene glycol, thus enabling the investigation of liquid crystalline properties of these concentrated suspensions. Using polarization microscopy and small-angle x-ray scattering (SAXS), self-organization into nematic and columnar mesophases is observed enabling the determination of the whole phase diagram as a function of ionic strength and rod volume fraction. When an external alternative electric field is applied, a very efficient orientation of the nanorods in the liquid-crystalline suspension is obtained, which is associated with a significant optical birefringence. These properties, combined with the high colloidal stability, are promising for the use of such high transparent and athermal material in electro-optical devices.

1. Introduction

Organic liquid crystals play an important role in many active devices such as displays which involve light transmission control using an external electric field. In the early 20th century, Zocher[1] demonstrated that liquid crystal (LC) behavior could also be observed on mineral suspensions of vanadium pentoxide ribbons. The pioneering theoretical work of Onsager[2] provided the explanation on the spontaneous nematic ordering of long hard rods in the purely entropic regime, opening a large field of investigation. In addition to fundamental issues related to self-organization of nanoparticles and their LC behavior, research on inorganic compounds opens the way toward devices that would take benefit from intrinsic properties of minerals such as large refractive index, absorption dichroïsm, ferroelectricity or ferromagnetism. Although still limited to a few number of compounds, some colloidal suspensions of anisotropic inorganic nanoparticles are now known to exhibit LC behavior such as nematic ordering, thus being referred to as mineral liquid crystals (MLCs).[3] During mainly the last decade, Rutile,[4] Boehmite,[5] Goethite[6] and CdSe/CdS quantum dots[7] in rod-like geometry, and Gibbsite,[8] Laponite and Bentonite[9] in shape of clay platelets have been the subject of numerous investigations. Those MLCs qualitatively follow the Onsager's theory, although van der Waals and electrostatic interactions between charged colloidal particles can make the real systems more complicated than the simple model of hard rods.[10]

In contrast to the vast use of organic LCs, practical applications of MLCs are still limited due to the difficulty in the synthesis of suspensions with appropriate properties up to high particle volume fraction. The question of the colloidal stability of anisotropic particles such as rods is of special importance considering that percolation threshold density ($\Phi_{percolation}$~ 0.7D/L where L and D are the length and the diameter of the rod, respectively[11]) which indicates that the gelation point of colloidal rods can occur below the spontaneous isotropic liquid–nematic (Iso-Nem) transition density ($\Phi_{iso\text{-}nem}$~ 4D/L) as predicted by Onsager.[2] Investigation of LC behavior over a wide range of Φ thus requires high inter-particle repulsion to avoid aggregation or gelation quenching the mobility of individual particles[12] which is essential for the collective LC behavior. Moreover, the dependence of the stability of colloidal systems on the suspension ionic strength have made it especially

J. Kim, Dr. R. Deloncle, Dr. K. Lahlil, Prof. J.-P. Boilot, Prof. T. Gacoin
Laboratoire de Physique de la Matière Condensée
CNRS–Ecole Polytechnique, 91128, Palaiseau, France
E-mail: thierry.gacoin@polytechnique.edu
A. de la Cotte, Dr. R. Deloncle, Prof. E. Grelet
Centre de Recherche Paul-Pascal
CNRS–Université de Bordeaux
115 Avenue Albert Schweitzer, 33600 Pessac, France
E-mail: grelet@crpp-bordeaux.cnrs.fr
Dr. S. Archambeau, Dr. C. Biver, Dr. J.-P. Cano
ESSILOR International
Rue Pierre et Marie Curie, 31682 Labège, France

DOI: 10.1002/adfm.201200825

difficult to electrically switch MLC orientation causing a short-circuit problem. Although different MLC systems have already been studied, there is thus still a place for research on new compounds with optimized properties in terms of LC behavior, dielectric contrast and anisotropy, and optical transparency, the latter concerning color and light scattering properties up to high volume fractions.

We here report a new type of MLC system composed of lanthanum phosphate ($LaPO_4$) nanorods stabilized in a non-aqueous solvent and totally free from aggregation. The excellent quality of suspensions obtained from an optimization of the process, attested by their limited light scattering properties, allowed us to investigate the LC properties even in the concentrated regime of the columnar mesophase. Nanorods with three different sizes were prepared to investigate the predicted effect of rod size on the LC behavior.[2] A phase diagram was established showing the stability of the different phases (isotropic liquid/nematic/columnar) as a function of the solution ionic strength. We finally showed the ability of these nanorod suspensions to be aligned both in the nematic and in the columnar phases by applying a weak external electric field, initiating further electro-optical investigations that had been one of the most undeveloped fields for MLCs.

2. Result and Discussion

2.1. Preparation of Colloidal $LaPO_4$ Nanorod Suspensions

Several previous works have reported on the synthesis of $LaPO_4$ particles with an anisotropic shape which is originated from the anisotropy of the crystallographic growth rate along the [001] direction.[13] The typical synthesis method is basically achieved in two steps: 1) precipitation of primary particles by mixing aqueous La^{3+} and PO_4^{3-} precursor solutions and 2) hydrothermal growth of these particles over 150 °C. As-prepared $LaPO_4$ particles are shown to exhibit a long rod-like shape when they were grown under acidic conditions (pH < 2). To our knowledge, there has been so far no report on the LC behavior of these colloidal $LaPO_4$ particles. This is presumably because of aggregation that usually occurs during or after the synthesis. Large rod aggregates are not appropriate for lyotropic LC behavior because they flocculate easily and scatter light enormously, resulting in an unstable colloidal suspension with turbid milky aspect.

We revisited the process and developed a simple method to produce individually dispersed $LaPO_4$ nanorod suspension avoiding aggregation even at high concentrations. As a starting point, we found out following the early developed methods[13] that, when the precursor solutions were mixed, instantly generated primary particles rapidly aggregated through some kind of oriented attachment mechanism leading to uncontrolled bundles and aggregates, and the following hydrothermal treatment thus leads to large rod aggregates (see Figure S1a in the Supporting Information). A key improvement could be obtained by limiting the aggregation of the primary particles by minimizing the concentration (down to 0.05 M) and the temperature (down to 0 °C) during the first step.[14] Importantly, the second step of hydrothermal treatment at 160 °C should be performed rapidly in order to enhance particle growth through dissolution/recrystallization process instead of aggregation. Following such a procedure, the dispersion quality and the colloidal stability of the product were greatly improved. (**Figure 1**a) shows a typical scanning electron microscopy (SEM) image of the as-prepared nanorods. The measured average length (L) and diameter (D) of the standard-sized rods (Figure 1a) are 252 nm and 11 nm respectively with an average aspect ratio (L/D) of 23. Monocrystalline structure is anticipated from the straight form with a constant diameter. This is confirmed by high-resolution transmission electron microscopy (TEM) image (Figure 1d) that clearly shows a periodic fringe pattern of lattice planes. The rod shape corresponds to the preferential growth along the **c** direction of the rhabdophane structure that was evidenced by powder X-ray diffraction (XRD) (Figure 1e).[13b–e]

Concerning the rod aspect ratio, which is an important parameter for the LC behavior, previous studies showed that it could be controlled by playing on the acidity of the medium during the synthesis.[13a] Nevertheless, this parameter could not be used considering that colloidal stability is only observed in a narrow pH range around 2 where the nanorod surface is strongly charged while the ionic strength is not too high. We then used another strategy considering that we found it possible to cut the standard rods using ultra-sonication. Samples with the same diameter (D = 11 nm) but shorter length (L = 200 nm) were obtained, corresponding to an aspect ratio of L/D = 18. A typical SEM image of these nanorods is shown in Figure 1b. This sample will further be referred to as lar-rods, considering their lower aspect ratio as compared to the standard rods (**Table 1**)

Finally, another route to obtain nanorods with different sizes was to let the primary particle suspension grow at ambient temperature instead of performing the hydrothermal treatment. In this case, we observed that crystallization of the particles into nanorods does occur slowly in several days leading to particles with almost the same aspect ratio as the standard-sized sample. As mentioned above, the overall quality of these samples is not as good as the one obtained after rapid hydrothermal treatment, but this was a way to obtain particles with a length about three times lower (L = 80 nm, D = 3.7 nm, L/D = 22) (Figure 1c, Table 1). These nanorods will further be referred to as s-rods, considering their smaller length as compared to the standard samples.

Colloidal stability of the aqueous $LaPO_4$ nanorod suspension can be maintained at pH < 3 and Φ < 1%. Flow-birefringence was observed in this state indicating the nanorod capability to self-organize into LCs. However, the dispersion equilibrium was easily broken out of this condition and typical instable kinetics such as flocculation or gelation took place as observed generally on various anisotropic inorganic colloidal systems.[11,12,15] Such a colloidal instability owing to aggregation disabled the system to exhibit spontaneous Iso-Nem phase transition that might have occurred at a higher Φ. Moreover, aging of the aqueous system was indispensible even at the pH and Φ range optimized for the initial colloidal stability: passing through a couple of months, aggregates were slowly generated making the suspension become turbid (Figure S1-2, Supporting Information). To avoid this unfavorable effect, MLCs have often been

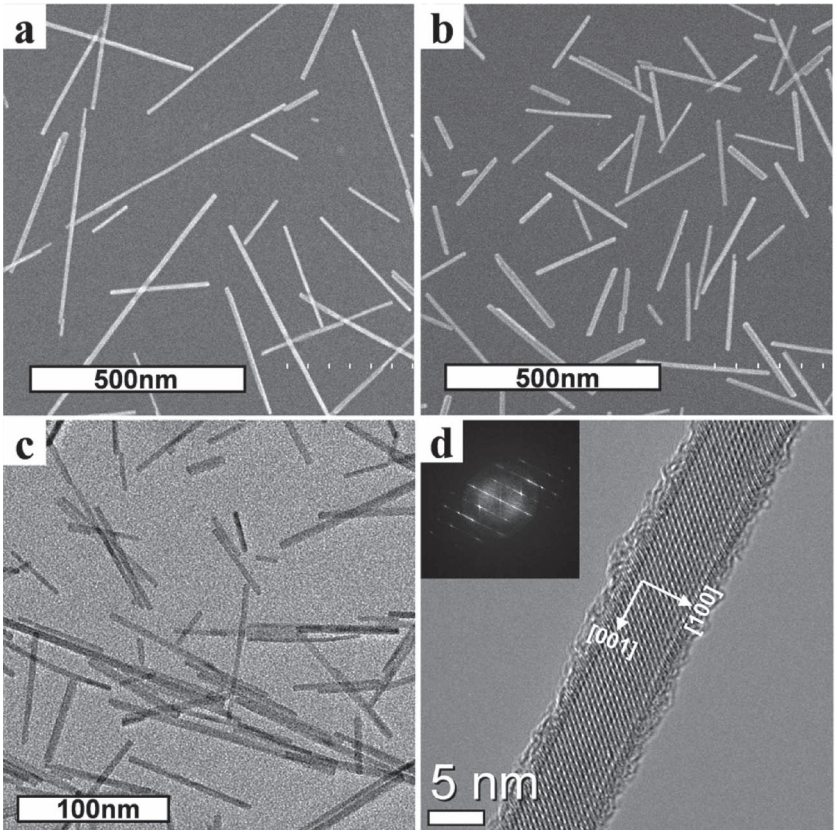

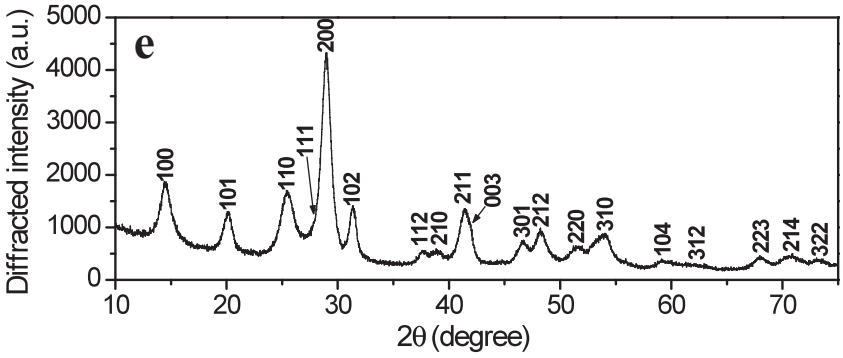

Figure 1. SEM images of standard rods (a) and lar-rods (b). c) TEM image of the s-rods. d) HR-TEM image of a standard rod. The white arrows indicate the crystallographic axis. Inset is the corresponding fast Fourier transformation (FFT). Note that the irregular surface is due to the fusion of the crystal by the high voltage electron beam for high resolution. e) XRD pattern of the standard rods and corresponding indexation from the rhabdophane reference (JCPDS 46-1439). Histograms of the size and diameter distributions on the three different-sized samples are given in Figure 2d,e and in the Supporting Information.

prepared by grafting polymeric molecules at the surface of rod-like particles to apply steric hindrance at the attraction domain.[5,16] But it is true that this way requires complex chemical routes and may change the original property of the colloidal system due to the large amount of molecules added into the system. Compatibility of the molecules with both the particle surface and the solvent should also be considered deliberately.

In a much more simple way, we were able to perfectly exclude aggregation and disclose pure LC property of $LaPO_4$ nanorods by exchanging the solvent from water to ethylene glycol (EG). EG is a polar protic solvent leading to the electrostatic stabilization of charged particles as in water. This is shown experimentally as the stability of the $LaPO_4$ particles is largely increased when EG is acidified to ensure the optimal surface charge, while the increase of the ionic strength by addition of salts decreases the dispersion stability. Furthermore, our experiments show that the stability in EG is significantly improved as compared to water, suggesting an additional effect of EG for the stabilization of the particles. The explanation has to be found in a specific interaction between glycol groups and the surface of the particles resulting in solvation and/or chelation of surface cations.[17] The presence of a capping shell of structured EG molecules may limit the minimal distance between particles providing the additional stabilization through steric hindrance. This appears similar to the common cases where polyethyleneglycol (PEG) is used to stabilize particles in water or biological media.[18] It should also be noted that the transfer is very easy, since EG is just added in the initial suspension and water is then removed by distillation. Actually, a permanent colloidal stability was achieved in EG over a large ionic concentration range at the elevated Φ where gelation dominated in the aqueous medium. As an evidence, a sample in EG with Φ = 6.2% (20.4 wt%) is showing a constant large transparency without any sign for aggregation during more than a few months (Figure S2, Supporting Information).

Table 1. Length, diameter, and aspect ratio of the different systems of $LaPO_4$ nanorods with their standard deviations (σ).

	L [nm]/σ	D [nm]/σ	*L*/*D*
standard-rods	252/0.63	11/0.19	23
lar-rods	200/0.64	11/0.23	18
s-rods	80/0.58	3.7/0.16	22

2.2. Liquid Crystalline Phase Behavior

Thanks to such an outstanding colloidal stability, two distinct liquid crystalline organizations at equilibrium have been observed from the $LaPO_4$ nanorods concentrated in EG. (**Figure 2**a,b) shows a macroscopically phase separated LC suspension of lar-rods concentrated in EG (Φ = 3.4%, before phase

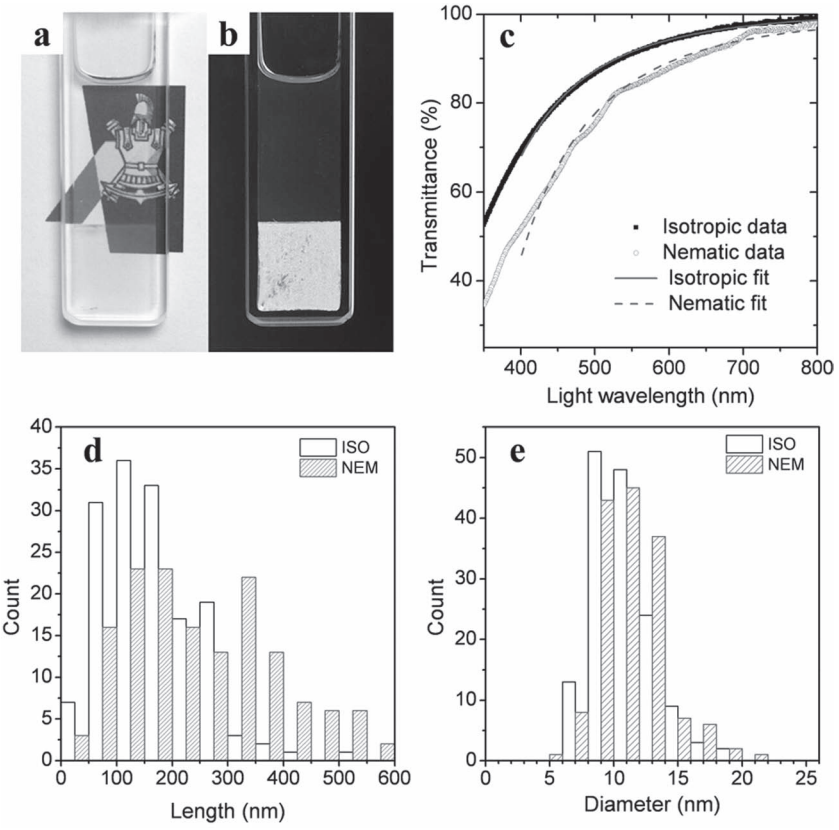

Figure 2. a) Macroscopic isotropic liquid–nematic (Iso-Nem) phase separation of $LaPO_4$ nanorod colloidal suspension in ethylene glycol. Both isotropic liquid upper state and nematic bottom state are transparent so that the figure behind the 2 mm-think cell is clearly seen. b) The same sample observed between crossed polarizers exhibits some birefringence associated with the nematic bottom phase. c) Transmittance spectra as a function of the light wavelength (λ) of both phases from the sample shown in (a,b). The transmittance T has been fitted according to the following equation $T = 1 - (\lambda_0/\lambda_4)$, characteristic of Rayleigh scattering. d,e) Nanorod length and diameter distributions measured in the isotropic and nematic phases respectively after macroscopic phase separation.

separation). The picture of the sample between crossed polarizer (Figure 2b) clearly shows the isotropic upper phase and the nematic bottom phase where some birefringence due to the randomly distributed nematic domains can be seen. This Iso-Nem macroscopic phase separation occurred only in one night after preparing the sample. Such a fast phase separation indicates that the LC behavior is not perturbed by other kinetic effects like gelation and that the system is very well stabilized in EG. This sample at the elevated Φ is transparent not only in the isotropic phase but also in the nematic phase (Figure 2a) indicating that aggregates were efficiently eliminated. Percent transmittance spectra in Figure 2c was taken directly from this cell, and the transmittances at 550 nm were 91% and 84% respectively for isotropic and nematic phases.

This indicates that, if it is used in the typical electro-optical devices with the thickness of several tens of micrometers, the light loss would be less than 1%. The transmission of the sample can be reasonably fitted with a $1/\lambda^4$ dependence, λ being the light wavelength. Such a behavior is typical of Rayleigh scattering. Note that some additional scattering exists in the nematic phase, probably due to the finite size of nematic domains. Size fractionation[2,19] which is predicted and observed on polydisperse systems, occurred in our system too. The size distribution histograms in Figure 2d,e shows that the isotropic phase contains more short rods (L = 163 nm, L/D = 16) and the nematic phase contains more long rods (L = 256 nm, L/D = 22).

Polarization microscopy enabled to directly observe and identify most of the different LC mesophases diluting the concentrated samples without waiting for the macroscopic phase separation. Highly birefringent texture of columnar mesophase, the Schilieren texture of the nematic phase, tactoids at the biphasic Iso-Nem range, and the dark isotropic liquid phase without birefringence are observed along the dilution and shown in **Figure 3**. Here, typical Schilieren texture and tactoids confirm again that our samples correspond to equilibrium states. Also, a phase diagram of the standard-sized nanorod sample as a function of the ionic strength and Φ was constructed (**Figure 4**) through the observation on the samples which were purified by a series of dialysis. The initial nitric acid concentration (C_{HNO3}) of the samples in EG with large Φ (up to 9%) was ~0.1 M. At such a high C_{HNO3}, the samples were in a turbid gel state due to the strong ionic strength–mainly given by C_{HNO3}, which counterbalances the repulsive surface charge resulting in particle aggregation (right dark region in Figure 4). Purification by dialysis effectively removes the nitric acid from those samples in the gel state. C_{HNO3} of once dialyzed samples decreased to ~0.02 M and they turned into a limpid LC mesophase sols. After a full purification, 99% of the nitric acid could be eliminated (C_{HNO3}~ 0.001 M). The non-diluted samples escaped from the gel state were purely nematic or even columnar as shown by X-ray scattering. And their successive dilutions showing various textures of LC mesophases (Figure 3) allowed us to find out the concentrations where the phase transition occurs.

According to the phase diagram (Figure 4), volume fractions for the Iso-Nem phase transition are much lower on the whole studied ionic strength range than the theoretical value ($\Phi_{iso\text{-}nem}$~17%) calculated by substituting the average rod aspect ratio (L/D = 23) into Onsager's theory of hard rods. However, electrostatic interactions have to be considered, by defining an effective rod diameter (D_{eff}), which is larger than the bare one and which depends on both the ionic strength of the medium and the particle surface charge density. Indeed, $LaPO_4$ nanorods are strongly positively charged in the acidic condition due to the surface protonation, which is in fact the driving force for the colloidal stability of the suspensions. Increasing ionic strength screens the repulsive electrostatic interactions, therefore revealing the bare particle dimensions by decreasing D_{eff}. The rod concentration scaling with the inverse of the effective

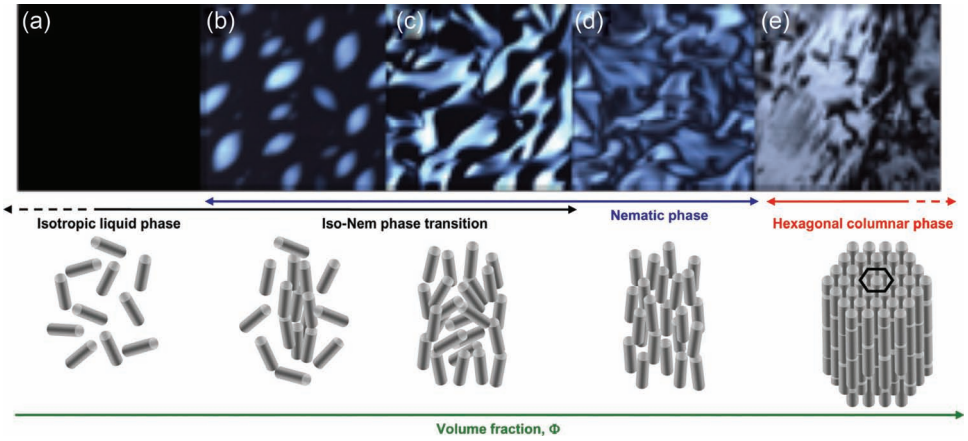

Figure 3. Optical texture observed by polarizing microscopy and schematic representation of the different liquid crystalline phases of $LaPO_4$ suspensions when increasing the nanorod volume fraction. a) Isotropic liquid phase appearing dark between crossed polarizers ($\Phi = 0.43\%$). b) Coexistence of both the isotropic liquid phase (dark background) and birefringent anisotropic droplets of the nematic phase (also called tactoids) ($\Phi = 0.92\%$) (image size: 220 µm). c) Sample at phase coexistence as picture (b) where the size of nematic regions has increased ($\Phi = 1.1\%$) (image size: 440 µm). d) Typical Schilieren texture of the nematic sample ($\Phi = 1.5\%$) (image size: 440 µm). e) Birefringent texture of a concentrated sample identified as a hexagonal columnar phase by small angle X-ray scattering (SAXS) ($\Phi = 4.34\%$) (image size: 1760 µm). Sample thickness is several micrometers for all microscopy images.

diameter, it is expected a shift to higher volume fractions of the Iso-Nem phase transition, as it is observed experimentally in Figure 4 (dashed lines). Moreover, the highest volume fraction for purely isotropic liquid $\Phi_{iso\text{-}max}$ of lar-rods (open triangles) with the low aspect ratio (L/D = 18) are placed higher than those of standard rods. These last two results show a qualitative agreement with Onsager's theory. The quantitative discrepancy with theory also observed in other MLCs[20] can be explained considering that the validity of Onsager's theory is for the needle-like limit, i.e., for rod aspect ratio $L/D >> 1$.[2] This is not the case of our $LaPO_4$ nanorods, especially when electrostatic interactions are taken into account by D_{eff}. Furthermore, rod polydispersity as well as attractive interactions can shift the volume fractions by broadening the biphasic domain at the Iso-Nem phase transition.[21] Such attractive interactions could originate from van der Waals interactions, which become effective at high ionic strength when electrostatic repulsions are screened. They can induce a transition from a sol to a gel state, as indicated in the right dark region in Figure 4.

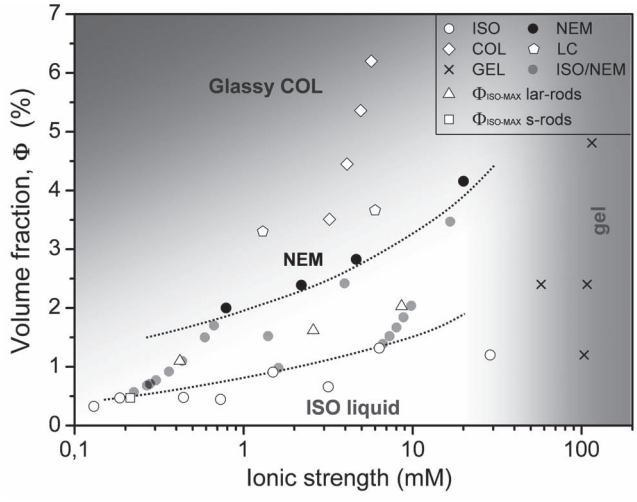

Figure 4. Phase diagram of $LaPO_4$ nanorod colloidal suspension in ethylene glycol. Open circles, black circles, and grey circles indicate isotropic, nematic, and isotropic/nematic biphasic domains of standard rods (L/D = 23) respectively. Open diamonds indicate columnar phase which were verified by SAXS, and open pentagons indicate purely liquid crystalline (nematic or columnar) domain of standard rods. Triangles indicate maximum volume fractions for purely isotropic phase ($\Phi_{iso\text{-}max}$) of lar-rods (L/D = 18) that are placed higher than those of standard rods. Open square is $\Phi_{iso\text{-}max}$ of s-rods (L/D = 22). Crosses indicate the high ionic strength domain where the suspension is in a gel state.

2.3. Small Angle X-Ray Scattering Analysis

An interesting feature of the concentrated suspensions is that their viscosity increased a lot during the purification process going toward the low ionic strength. They finally turned into a glassy-like state (Upper left dark region in Figure 4) which corresponds to a hexagonal columnar mesophase as demonstrated by small angle X-ray scattering (SAXS) in **Figure 5**. In this highly ordered phase, the nanorods self-organize into liquid-like columns which in turn form a bi-dimensional hexagonal crystalline array (Figure 3). In this phase at low ionic strength, repulsive interactions dominate, therefore avoiding particle aggregation and maintaining a large transparency of the suspension. For this reason, the pure LC phases of the $LaPO_4$ system can be manipulated in the concentrated regime. It is sometimes difficult to distinguish unambiguously by polarization microscopy the nematic phase from the columnar one - because both mesophases are birefringent. Several points above the Iso-Nem biphasic range on the phase diagram (Figure 4) are thus still unclear whether they are in nematic or in columnar phase. Instead, SAXS experiments have been performed for

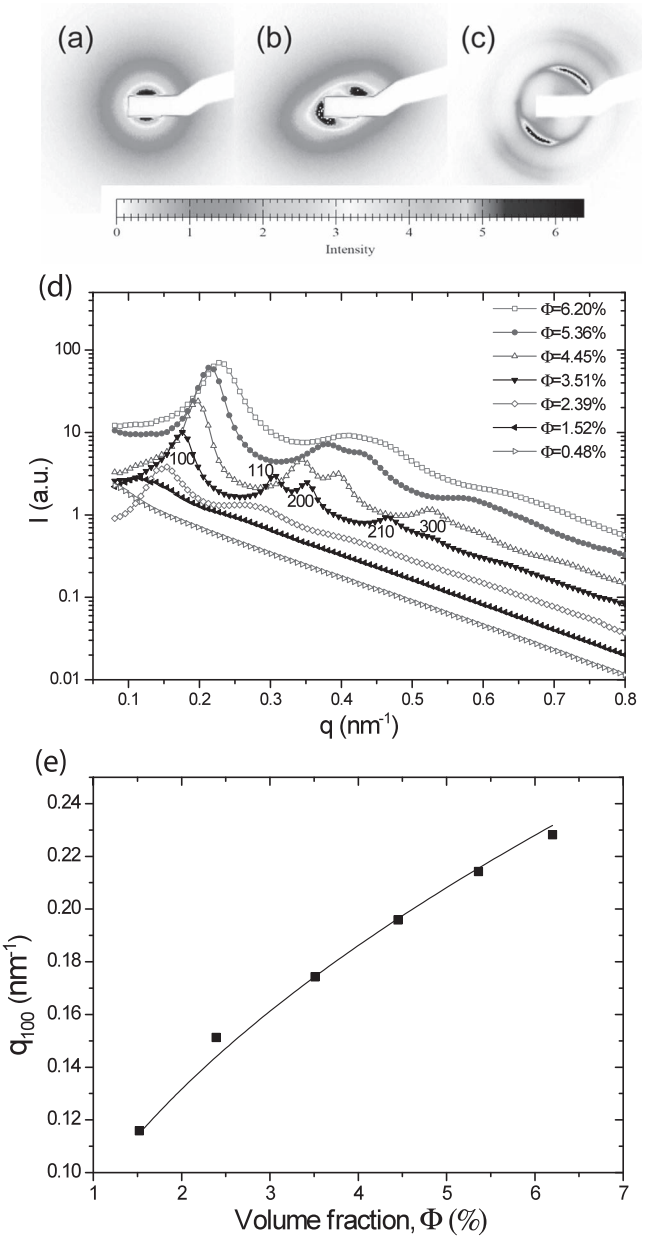

Figure 5. Typical diffraction patterns obtained by SAXS in a) the isotropic liquid phase, b) the nematic phase, and c) the columnar phase. d) Scattered intensity *I* as a function of the wave vector q for different volume fractions Φ of $LaPO_4$ suspensions. The Miller indices only shown for clarity at $\Phi = 3.51\%$ indicate a hexagonal structure of the columnar mesophase. e) Evolution of the position of the main Bragg reflection (100) with the nanorod volume fraction Φ. The dark line is a data fit $q_{100} = \alpha\Phi^{1/2}$ characterizing a swelling law of a 2D order.

different dilutions of one purified sample (Figure 5d), indicating a swelling law behavior of bi-dimensional order with $q_{100} = \alpha\Phi^{1/2}$ (Figure 5e). The prefactor α can be easily calculated for a hexagonal lattice with $\alpha^2 = 32\pi/(\sqrt{3}D^2)$. From the numerical fit of the data, the rod diameter can be estimated as approximately 8 nm, which is roughly consistent with the value of 11 nm measured by SEM (Table 1). Note that some broadening of the Bragg reflections can be seen in the columnar range by increasing the rod volume fraction (Figure 5d). This is related to finite size effects originating from the concentration step of the particles, in which the LC domain size in the sample decreases by removing the solvent, increasing therefore the width of the Bragg peaks.[22]

2.4. Alignment Under Electric Field

Considering the outstanding colloidal stability and the good optical transparency at low ionic strength even for high Φ of particles, this system appears very attractive for investigations of electro-optical properties targeting active transparent devices. Experiments were achieved both on a nematic phase at $\Phi = 1.55\%$ and on a columnar phases at $\Phi = 4.34\%$ respectively, at low ionic strength, in an experimental cell made of an ITO electrode with a gap and a glass coverslip. Typical birefringent texture was observed initially, where the LC domains were randomly oriented at the macroscopic scale (**Figure 6**a). When the electric field was applied, the nanorods on the gap were aligned along the electric field inducing a bright birefringence on this area where the orientational order parameter (*S*) is close to 1 for $E > E_S$ (Figure 6b). When the electric field was turned off, the macroscopic alignment - free of topological defects - is conserved because no elastic force exists to restore the initial random alignment (Figure 6c). The value of *S* by spontaneous orientation without electric field is less than the one driven by electric field, therefore it relaxed back in about 1 hour resulting in a decrease of the birefringence. Quantitative measurements of the orientation and the relaxation of the LC phases by an electric field are shown in Figure 6d,e. Interestingly, the critical field required to fully orient both the nematic and the columnar phases is found to be quite low ($E_S \sim 0.05$ V/μm). It must be noted that in these experiments, the initial values of the birefringence (at zero field) depends on the arbitrary orientation of the domain where the measurement is made. The final value of the birefringence (4.4×10^{-3}) must be considered relatively to the volume fraction of nanoparticles ($\Phi = 4.34\%$). Assuming a linear relationship, extrapolation of this value for $\Phi = 100\%$ gives a normalized birefringence of about 0.1, which is comparable to pure compounds of typical thermotropic LCs. The long relaxation time is also peculiar as this enables to maintain the once switched state for a long while after turning the field off. Thus a promising electro-optical performance is clearly demonstrated in our system, being therefore one of the first mineral LCs for which the effect of applied electric field can be easily investigated.[23,24] Application of this material to a switchable optical device would also benefit from its low production cost compared to expensive organic LC compounds and the distinguished properties of the mineral colloidal system such as athermal LC behavior and stability of the mineral mesogens under irradiation of UV or large flux of light. This could be used for different practical applications such as smart windows or high power laser modulation over a large range of light wavelength including UV. Further experiments such as inducing a birefringent nematic phase

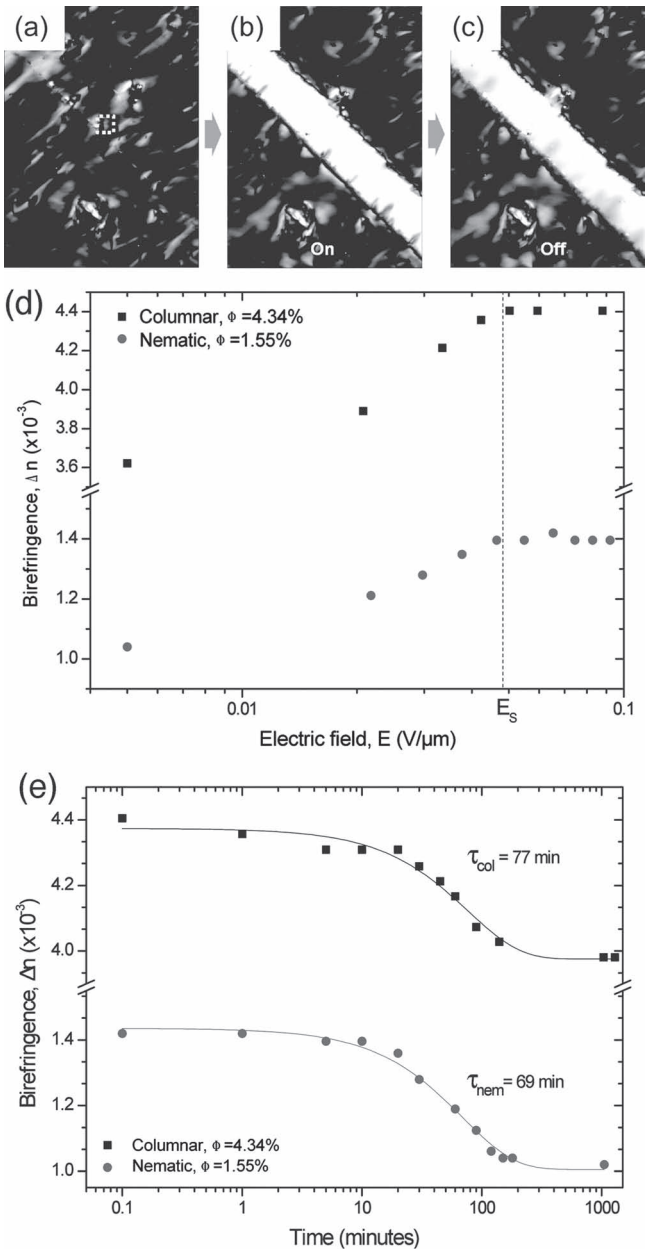

Figure 6. Optical microscopy images of the $LaPO_4$ nanorod colloidal liquid crystalline suspensions deposited in a cell of about 45 μm thick. This cell is made by a glass coverslip and an ITO electrode with a gap width of 170 μm has been performed for applying an alternative in-plane electric field, *E*. a) Before applying the electric field, the samples exhibit some birefringent domains. Dashed box indicates the zone where the birefringence was measured using Berek compensator. b,d) The application of a sinusoidal electric field at a frequency of 400 kHz induced the orientation of the (nematic or columnar) mesophase in the gap showing large birefringence. c,e) When the electric field is switched off, relaxation of the nanorod alignment is observed with a decrease of the associated birefringence. This corresponds to an exponential decay with a characteristic time τ of about 1 h in both phases, as shown by the solid lines in panel (e).

by an electric field from the isotropic liquid phase (also called Kerr effect)[25] can be envisaged in near future with our colloidal $LaPO_4$ nanorod suspensions.

3. Conclusions

In this work, we have shown that $LaPO_4$ nanorods dispersed in ethylene glycol exhibit a very high colloidal stability in suspension, as shown by the self-organization into different liquid crystalline phases, e.g., nematic and columnar mesophases. These stable dispersions have been obtained through the optimization of the whole process of synthesis, solvent transfer, and purification, but without any specific chemical functionalization of the nanorod surface. This enables therefore production of large amount of such nanorod suspension in a few steps, and it could possibly be applicable for other mineral colloidal systems. We have also shown that these concentrated nanorods dispersions can be very efficiently aligned with a weak applied electric field of about 0.05 V/μm, exhibiting then relatively large optical birefringence at low volume fraction. Associated with a high optical transparency, this opens the way toward electro-optical devices based on mineral liquid crystals.

4. Experimental Section

Preparation: Equimolar (0.05 M) solutions of $La(NO_3)_3$ and $(NH_4)_2HPO_4$ were mixed at 0 °C, and the mixture was rapidly heated to 160 °C in the autoclave to produce grown $LaPO_4$ nanorods. Lar-rods were prepared by doing ultrasonication during 3 h on the grown nanorods suspension. S-srods were prepared by leaving the precursor solution mixture stirred during 4 days at the ambient temperature without hydrothermal treatment. So-prepared aqueous colloidal suspensions were washed once by centrifugation, and then purified by dialyzing in 0.01 M aqueous nitric acid solution to remove residual reactive ions. Purified nanorods were then transferred into ethylene glycol (EG) by mixing with EG and then distilling water using rotary evaporator. The volume fraction (Φ) of nanorod suspensions were also modified here by varying the mixed EG volume. Purification by dialysis in EG was conducted four times in series refreshing the EG bath.

Chracterization: High resolution transmission electron microscopy (TEM) and scanning electron microscopy (SEM) were performed respectively on FEI Tecnai F20 and Hitachi S4800 field electron gun scanning electron microscope (FEG-SEM). To identify the extent of aggregates, SEM samples were prepared by attaching nanorods on a negatively charged poly-styrene-sulphonate layer coated on a silicon wafer substrate. The nanorod size data were obtained by counting the length and diameter of 300 individual particles on different SEM images (for standard rods and lar-rods) and TEM images (for s-rods) from each sample. The estimated precision for the size determination is about 1 nm for standard rods and lar-rods, and about 0.2 nm for s-rods respectively. X-ray diffraction (XRD) pattern was obtained using Philips X'pert diffraction system working at CuKα radiation, and indexed comparing with the rhabdophane reference -JCPDS 46-1439. Small angle X-ray scattering (SAXS) measurements were carried out on the SWING beamline at the synchrotron radiation facility SOLEIL (France), with a sample to detector distance of 1384 mm and with a wavelength of 0.103 nm. The polarization optical microscopy to observe the LC texture and to perform the electro-optical measurements was conducted on 15 μL of $LaPO_4$ suspensions deposited between a typical microscope slide and a coverslip using Olympus BX51 microscope combined with a color CCD camera (JAI, CV-M7). Indium tin oxide (ITO) electrodes with a gap of about 170 μm width were connected to a function generator for applying an in-plane sinusoidal alternative electric field on $LaPO_4$ suspensions. Birefringence measurements were performed locally in the sample, typically in a 50 μm × 50 μm zone by using a Berek compensator providing the optical retardation. An equilibration time of 2 min was taken between two measurements under applied electric field. Nitric acid concentration (C_{acid}) was obtained by fitting the measured

electric conductivity (σ) to the C_{acid} vs. σ curve of the reference nitric acid solutions. The mass concentration of the colloidal solution was obtained with a dried sample of a given volume, and the volume fraction was calculated dividing it by the density of $LaPO_4$ in rhabdophane phase, 4.3 g/cm^3.

Supporting Information

Supporting Information is available from the Wiley Online Library or from the author.

Acknowledgements

The authors would like to thank F. Nallet and L. Navailles for the synchrotron beamtime. S. Bellei, A. Potdevin and R. Tricarico are acknowledged for preliminary experiments.

Received: March 23, 2012
Revised: May 22, 2012
Published online: July 23, 2012

[1] H. Zocher, *Z. Anorg. Allg. Chem.* **1925**, *147*, 91.
[2] L. Onsager, *Ann. N.Y. Acad. Sci.* **1949**, *51*, 627.
[3] a) P. Davidson, J.-C. P. Gabriel, *Curr. Opin. Colloid Interface Sci.* **2005**, *9*, 377; b) J. C. P. Gabriel, P. Davidson, *Adv. Mater.* **2000**, *12*, 9.
[4] A. Dessombz, D. Chiche, P. Davidson, P. Panine, C. Chanéac, J.-P. Jolivet, *J. Am. Chem. Soc.* **2007**, *129*, 5904.
[5] P. A. Buining, H. N. W. Lekkerkerker, *J. Phys. Chem.* **1993**, *97*, 11510.
[6] B. J. Lemaire, P. Davidson, J. Ferré, J. P. Jamet, P. Panine, I. Dozov, J. P. Jolivet, *Phys. Rev. Lett.* **2002**, *88*, 125507.
[7] L.-s. Li, J. Walda, L. Manna, A. P. Alivisatos, *Nano Lett.* **2002**, *2*, 557.
[8] F. M. van der Kooij, H. N. W. Lekkerkerker, *J. Phys. Chem. B* **1998**, *102*, 7829.
[9] J.-C. P. Gabriel, C. Sanchez, P. Davidson, *J. Phys. Chem.* **1996**, *100*, 11139.
[10] A. Stroobants, H. N. W. Lekkerkerker, T. Odijk, *Macromolecules* **1986**, *19*, 2232.
[11] A. P. Philipse, A. M. Wierenga, *Langmuir* **1998**, *14*, 49.
[12] a) A. Mohraz, D. B. Moler, R. M. Ziff, M. J. Solomon, *Phys. Rev. Lett.* **2004**, *92*, 155503; b) M. J. Solomon, P. T. Spicer, *Soft Matter* **2010**, *6*, 1391; c) A. Wierenga, A. P. Philipse, H. N. W. Lekkerkerker, D. V. Boger, *Langmuir* **1998**, *14*, 55; d) A. Mohraz, M. J. Solomon, *J. Colloid Interface Sci.* **2006**, *300*, 155.
[13] a) H. Meyssamy, K. Riwotzki, A. Kornowski, S. Naused, M. Haase, *Adv. Mater.* **1999**, *11*, 840; b) Y.-P. Fang, A.-W. Xu, R.-Q. Song, H.-X. Zhang, L.-P. You, J. C. Yu, H.-Q. Liu, *J. Am. Chem. Soc.* **2003**, *125*, 16025; c) X. Wang, M. Gao, *J. Mater. Chem.* **2006**, *16*, 1360; d) W. Bu, L. Zhang, Z. Hua, H. Chen, J. Shi, *Cryst. Growth Des.* **2007**, *7*, 2305; e) M.-G. Ma, J.-F. Zhu, S.-W. Cao, F. Chen, R.-C. Sun, *J. Alloys Compd.* *492*, 559.
[14] a) M. Y. Lin, H. M. Lindsay, D. A. Weitz, R. C. Ball, R. Klein, P. Meakin, *Nature* **1989**, *339*, 360; b) P. Van der Schoot, *J. Phys. Chem.* **1992**, *96*, 6083.
[15] V. Trappe, P. Sandkühler, *Curr. Opin. Colloid Interface Sci.* **2004**, *8*, 494.
[16] a) M. P. B. van Bruggen, H. N. W. Lekkerkerker, *Langmuir* **2002**, *18*, 7141; b) S. Meuer, P. Oberle, P. Theato, W. Tremel, R. Zentel, *Adv. Mater.* **2007**, *19*, 2073.
[17] P. Yang, Z. Quan, C. Li, Z. Hou, W. Wang, J. Lin, *J. Solid State Chem.* **2009**, *182*, 1045.
[18] A. Mpandou, B. Siffert, *Colloids Surf.* **1987**, *24*, 159.
[19] G. Oster, *J. Gen. Physiol.* **1950**, *33*, 445.
[20] P. Davidson, *C. R. Chim.* **2010**, *13*, 142.
[21] G. J. Vroege, H. N. W. Lekkerkerker, *Rep. Prog. Phys.* **1992**, *55*, 1241.
[22] E. Grelet, *Phys. Rev. Lett.* **2008**, *100*, 168301.
[23] E. Paineau, K. Antonova, C. Baravian, I. Bihannic, P. Davidson, I. Dozov, M. Imperor-Clerc, P. Levitz, A. Madsen, F. Meneau, L. J. Michot, *J. Phys. Chem. B* **2009**, *113*, 15858.
[24] M. Zorn, M. N. Tahir, B. Bergmann, W. Tremel, C. Grigoriadis, G. Floudas, R. Zentel, *Macromolecules* **2010**, *31*, 1101.
[25] I. Dozov, E. Paineau, P. Davidson, K. Antonova, C. Baravian, I. Bihannic, L. J. Michot, *J. Phys. Chem. B* **2011**, *115*, 7751.